

---

# Evaluation of reflectivity of metal parts by a thermo-camera

Zoltán Sárosi, Wolfgang Knapp, Andreas Kunz, Konrad Wegener  
IWF, ETH Zurich, Switzerland

---

## ABSTRACT

All objects, apart from black-bodies, reflect a part of the incident radiation. The reflected fraction of incident radiation is termed as 'reflectivity'. The reflectivity of surfaces is often a function of the wavelength, the material, the quality of the surface, and the incident angle of the radiation. In order to evaluate the specular reflectivity of a surface at small incident angles, a method, based on thermal radiation measurement by a thermo-camera, was developed. A quasi black-body, a so-called 'Hohlraumstrahler', was realized and used as thermal radiation source. The temperature of the source was continuously monitored by temperature probes at 3 different locations inside the source, while the radiation flux of the source was measured by a thermo-camera. During a calibration process, the temperature data from the probes and the radiation flux measured by the thermo-camera were simultaneously recorded and evaluated. In a next step, the radiation from the source was reflected by the samples and measured by the thermo-camera along with the temperature data from the probes. Using the calibration data, the reflected radiation flux could be calculated. The surface profiles of the samples were also measured by a stylus instrument. The calculated reflectivities were evaluated together with the surface roughness of the samples. The results showed good coincidence with the theoretical model of Bennett and Porteus [1].

## INTRODUCTION

Reflectivity refers to the fraction of the incident electromagnetic power that is reflected from a surface. The reflected irradiation consists of a scattered or diffuse and specularly reflected part. The scattered irradiation is distributed in every direction in a hemisphere ( $2\pi$  solid angle) over the surface, while the specularly reflected part terms only the irradiance in a single direction, which is defined by the law of reflection.

In order to assess the specular reflectivity of a surface in the MWIR (Medium Wave Infrared) spectrum, and evaluate how it is influenced by the surface roughness, a simple measurement method was elaborated. For the measurement of surface reflectivity a calibrated radiation source and detector are required, usually lasers and special detectors are used for this purpose. The laser beam points at the surface in question, from which it is reflected and scattered, and then the scattered beam is captured by a detector. The power of the incident and irradiant radiation is measured, and their quotient gives the reflectivity.

The detectors usually have only one sensor element, hence they are not position sensitive, meaning that the whole surface of the detector measures a single intensity value. The detector has to be placed precisely in the center of the scattered beam, where the intensity is maximal. Placing the detector to the appropriate position can be difficult, due to the invisible character of the laser beam. The invisible laser beams can be made visible in a given plane by the help of a special indicator sheet that change its color if being illuminated by an intense laser beam. This way, the path of the beam can be followed by placing the indicator in the beam's path. It is though not always straightforward, especially in case of rough surfaces which scatter the incident beam in a large degree, decreasing the intensity of the radiation falling onto the indicator.

Using a thermo camera, the spectrum, invisible to the human eye, can be observed on a display, making the positioning of the specimens easier. Unfortunately, the reflected laserbeam cannot be directly observed by a camera, only if it is scattered from a Lambertian scatterer like a white paper sheet that evenly distributes the incident radiation in all directions [4]. Instead of a thin laser beam, a simulated black-body radiation source can be used that emits radiation in a wide angle.

## THEORETICAL MODEL

There are several models in the literature that describe the reflection of the light on a surface in function of the surface parameters and the wavelength of the light. Some of these models are very complex like the He-Torrance-Sillion-Greenberg model [2], that generates physically correct results for a wide parameter range: all incident and reflection angles, different surface qualities, different polarization directions. There are some

simpler models, like the one from Bennett and Porteus [1] that works well under limited conditions: near perpendicular incident and observation direction and limitations on the surface quality. The hypothesis according to [2] predicts the reflectivity of conducting metallic surfaces at near incident angle in the following way:

$$\sigma = \sigma_0 \exp\left(-\frac{(4\pi R_q)^2}{\lambda^2}\right) + \sigma_0 \frac{2^5 \pi^4}{R_{\Delta q}^2} \left(\frac{R_q}{\lambda}\right)^4 (\Delta\theta)^2 \quad (1)$$

Where  $\sigma$  is the reflectivity,  $\sigma_0$  is the reflectivity of a perfectly smooth surface of the same material,  $\lambda$  is the wavelength of the radiation used for the investigation,  $R_q$  is the RMS-roughness (Root Mean Square) of the surface,  $R_{\Delta q}$  is the RMS-slope of the surface,  $\Delta\theta$  is the instrumental acceptance angle. It can be seen from Equation 1, if the wavelength of the light ( $\lambda$ ) is sufficiently long relative to  $R_q$ , then due to  $\left(\frac{R_q}{\lambda}\right)^4$ , Equation 1 reduces to:

$$\sigma = \sigma_s = \sigma_0 \exp\left(-\frac{(4\pi R_q)^2}{\lambda^2}\right) \quad (2)$$

where  $\sigma_s$  is the specular reflectance. The critical length of the wavelength is defined by the Rayleigh criterion:

$$R_q < \frac{\lambda}{8 \cos \theta} \quad (3)$$

where  $\theta$  is the incident angle. If the wavelength of the light is much longer than the height irregularities of the surface, the surface scattering will be negligible and the surface can be considered to be smooth at the given wavelength, thus Equation 2 can be used for the calculation of the specular reflectance.

It can be seen from the above equations, that the reflectivity depends on both the microstructure of the surface ( $R_q$ ) and the material as well ( $\sigma_0$ ). In Figure 1, the spectral reflectivity ( $\sigma_0(\lambda)$ ) of different perfectly smooth metal surfaces is shown. It can be seen, that reflectivity of the perfectly smooth metal surfaces is generally higher in the MWIR than in the visible spectrum, and it converges to 1 with the increasing wavelength.

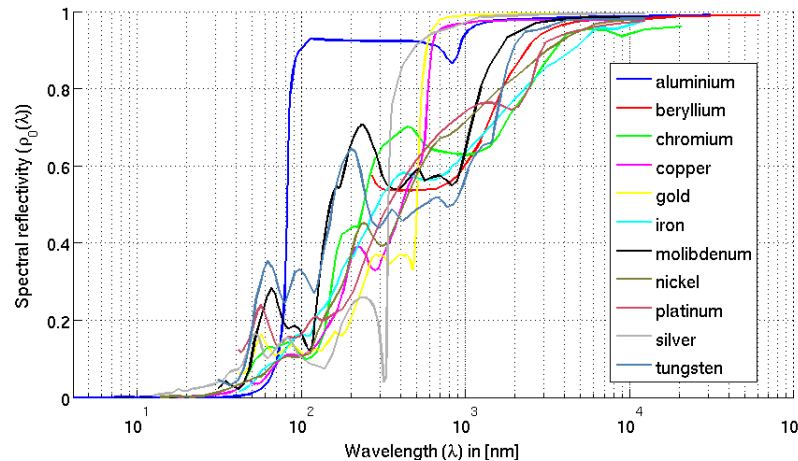


Figure 1: Spectral reflectivity of perfectly smooth metal surfaces [3]

There are though some conditions, which should be fulfilled in order to get accurate results:

- Gaussian height distribution of surface irregularities
- Gaussian distribution of the autocovariance function of the surface irregularities
- Stationary and ergodic surface
- Parallel incident light beam
- Monochromatic radiation
- Normal angle of incidence

Unfortunately, in case of our measurements some of these conditions are not fulfilled, thus some deviations between the measured and the calculated results are expected.

**TEST OBJECTS**

For the measurements, we used several different test objects from two different materials: hardened steel and aluminum. The specimens differed not only in material, but also in the surface quality. We tested several sheet metal and machined surfaces: like plane ground, filed and milled. For studying different surfaces made from the same material, machined with the same machining process, but with different surface roughnesses the so called Rugotest specimens are a good choice. In Figure 2 a Rugotest object can be seen, the different sections on the object were all plane ground, but they are all in a different surface roughness class (from N1 to N8:  $R_a = 0.025\mu\text{m} - 3.2\mu\text{m}$ ).

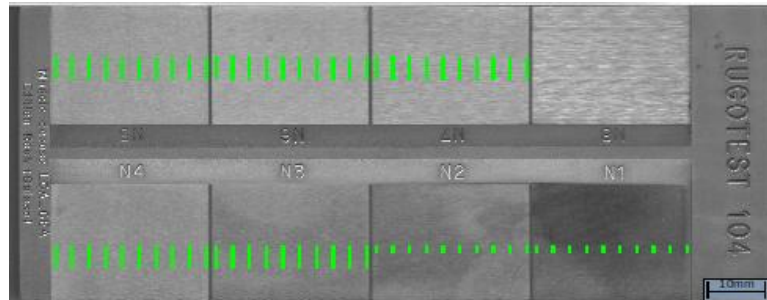


Figure 2: Image of a plane ground “Rugotest” part. The thin green lines mark the roughness profile measurement paths.

**SURFACE ROUGHNESS MEASUREMENTS**

The surface profile of each test surface was measured by a Rank Taylor Hobson Talysurf series stylus type measurement device. Each test surface was measured at 10 different positions, along 10 short linear sections distributed uniformly on the object’s surface along an axis that is perpendicular the measurement sections (see Figure 2). The measurements were made in direction perpendicular to the machining grooves of the surface. The individual measurements were processed by the Talysurf software according to the ISO standard 4288 [5]. The resulted surface profiles were further processed in MATLAB (see Figure 3a), by which the different roughness parameters like the RMS-roughness ( $R_q$ ), the RMS-slope ( $R_{\Delta q}$ ) and autocovariance length ( $\tau$ ) were calculated. For each surface, a mean  $R_q$  value and a deviation range was calculated and used for the later evaluation.

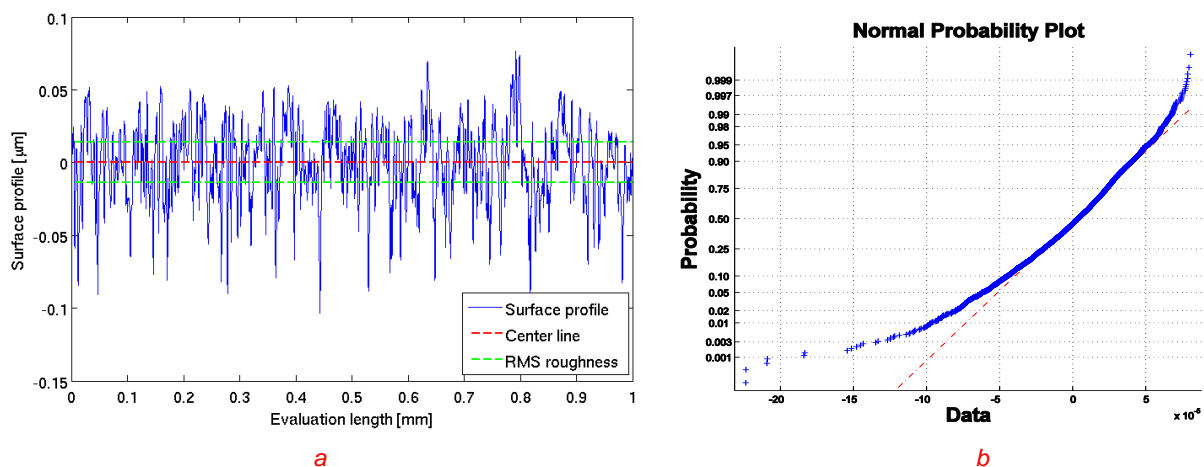


Figure 3: a: Surface profile of a test object, b: normal probability plot

The distribution of the height irregularities and the autocovariance functions were also evaluated for each surface profile. We found that none of these distributions was perfect Gaussian. In Figure 3b, the normal probability plot shows the deviation of a surface from the ideal Gaussian distribution.

## MEASUREMENT SETUP

The measurement setup can be seen in Figure 4, it consists of a thermo camera and a radiation source, that are attached to a mount, which allows to easily set the angle and the distance of the source and the camera ( $\theta_i, \theta_r, d_i, d_r$ ) as well the rotation angle ( $\omega_o$ ) and the distance of the object ( $h_o$ ).

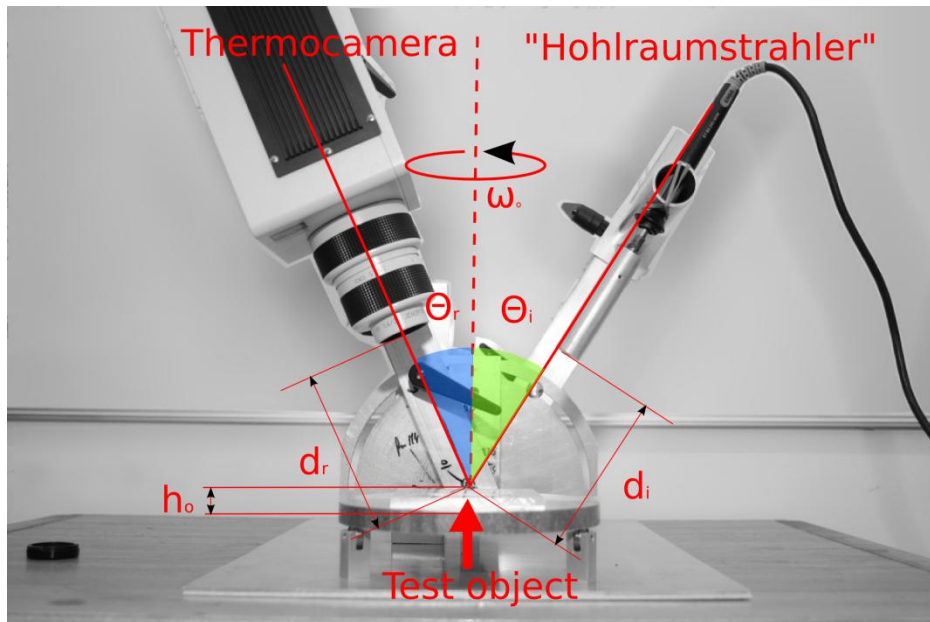


Figure 4: Measurement arrangement

## THERMOCAMERA

For the measurements, a VarioTherm Head II thermocamera was used. This model has a FPA (Focal Plane Array) detector, consisting of (256x256) PtSi-sensor elements. The working spectrum of the camera is in the MWIR range, between 3.4 $\mu$ m and 5 $\mu$ m wavelengths. For the measurements the standard 25mm lens was used, providing a 14°x14° field of view.

## RADIATION SOURCE

As it was mentioned before, the reflectance is a quotient of the power of the incident and the reflected radiation; it is not an attribute that can be directly measured. A radiation source that fulfills the following requirements is required for the reflectance evaluation:

- Considerable portion of the radiation has to be in the spectral range of the detector (MWIR)
- Simulated black-body: minimal or no reflection, no transparency, maximal or full emission
- Optimal physical dimensions
- Constant radiant exitance

A simple simulated black-body, a so-called “Hohlraumstrahler”, that emits electromagnetic radiation at the whole spectrum, while having a minimal reflectivity and zero transparency, was constructed. The source was a cylindrical bolt made from aluminum, with two larger drills at the two ends and six smaller drills on the side along one of the larger drill (see Figure 5). Temperature probes were inserted in the small drills that measured the temperature of the source during the tests. In one of the larger drills a heating element, an 80W soldering iron was inserted, heating the whole source to a temperature of 300°C. The other large drill was the source of the thermal radiation. In practice, a narrow and deep cavity can be considered as a “Hohlraum” that is a simulated black-body, if the cross section of its opening is small relative to its depth, often 1:4 ratio is used as a rule of thumb. Our source had a cross section of 7mm and a depth of 35mm, making a 1:5 ratio. In order to further increase the emissivity of the source and reduce its reflectivity, its inner surface was painted with heat resistant black matte lacquer that has an emissivity of 0.97 according to [6,7]. The emissivity of the simulated black-body can be calculated using the Gouffé method [6] if the dimensions of the cavity and the emissivity of

the surface paint are known, which results in our case in 0.91, which indicates that our source is not quite a real black-body that would have a theoretical emissivity of 1. In order to reduce unwanted reflectivity of the area around the cavity, it was painted with chalk spray, giving a white diffuse surface finish. Better results could be reached by the application of a thermally decoupled aperture, which has a deeper temperature than the source object in front of the cavity.

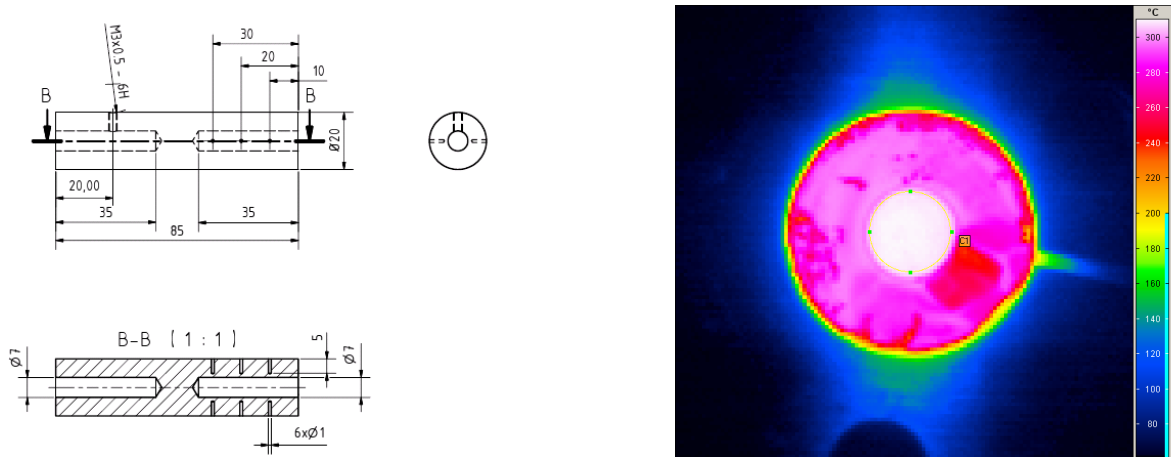


Figure 5: CAD drawing of the radiation source and its thermo camera image

The following two dimensions of the source had to be optimized: thermal capacity and the surface area of the radiating spot. The thermal capacity of the source depends on the material and the mass - which depends on the dimensions - of the body. Low thermal capacity results in higher instability in the temperature, on the other hand a high thermal capacity would lower the maximal reachable temperature and would elongate the time required to reach the maximal temperature in case of a given heating element.

Another important factor that influences the dimensions of the source is the area of the opening through which the most intensive radiation leaves the source. The size of the “Hohlraum” drill was optimized by two factors: solid angle that is visible from the objects position, and number of pixels it occupies in the camera image. The larger the solid angle of the source is, the larger the diffuse or scattered part of the irradiance is that is added to the specular reflection. The minimal area of the radiating spot is limited by the lateral resolution of the detector and its distance to the measured spot. If the radiating spot is too small, only a few detector pixels are taking part in the measurements, resulting in higher instability of the measured radiation, because of the noise of the individual detector pixels. The larger the opening is, the more pixels are taking part in the measurement and the noise of the individual pixels is compensated if a mean value of all triggered pixels is calculated (see Figure 5). With a smaller measurement spot, the portion of the detector pixels that are receiving radiation on only a part of their surface is also larger, which increases the measurement noise, and the accuracy of the pixels. If the surface of a detector pixel is not fully covered by the radiation, the accuracy of the detected radiation is lower (for more details see [8]). On the other hand, if the size of the radiating spot is too large, it raises the portion of the diffuse reflection on the measured surface since the radiation is coming from a larger solid angle.

### TEMPERATURE MEASUREMENT

For the reflectance measurement, both the radiant exitance of the source and the irradiance from the test object have to be measured simultaneously, since their quotient defines the reflectivity. Unfortunately, both of them cannot be measured at the same time with only one camera, since the source is directed to the test surface, and the camera cannot have both, the direct and the reflected view of the cavity at the same time. If the radiation source could provide a constant radiant exitance, it could be measured once before the reflectance measurements, and used later for the calculations. Unfortunately, the temperature of the source slightly varies. Since the radiant exitance, according to the Stefan-Boltzmann law, is proportional to the 4<sup>th</sup> power of the temperature, it could influence the measured radiant exitance to a considerable degree. The solution for this problem is to directly measure the temperature of the source by temperature probes in the

body of the source, near the “Hohlraum”, and calculate the radiant exitance, based on a calibration prior to the measurement.

The temperature of the source was measured by three temperature probes at different positions inside the body of the source nearby the “Hohlraum” drill (see Figure 5). The temperature probes were attached to a computer through three thermo elements. The computer registered the temperatures of the three probes at a 1Hz rate, and created a datafile.

**EVALUATION OF THE MEASURED DATA**

The measured data from the two different sources: thermo camera and temperature sensors were processed in MATLAB. The temperature sensor data and the thermo images were recorded simultaneously by two different systems, thus the corresponding records from the two different datasets had to be found. The clocks of the two systems were synchronized previously. The time stamps of the two datasets’ elements were compared and paired with the corresponding record from the other dataset.

The thermo camera measures temperature values with a given accuracy as long as the measured value is in the calibration range. If the measured temperature is out of the calibration range, the measurement has a very high inaccuracy. Thus, each recorded thermo camera image had to be examined, and dropped if it contained measured points exceeding the calibration range, but only in those areas that were relevant to the measurement. The images from the thermo camera were first processed by the camera’s software in order to have each thermogram in two different units: Celsius and Watt/m<sup>2</sup>; Celsius is needed to control the violation of the calibration range, and Watt/m<sup>2</sup> is required for the reflectance evaluation. The data was exported in both units in ASCII format that can be processed by MATLAB. The images with measurement values outside the calibration range are dropped based on their Celsius data, after this step the Celsius data is no longer needed, the work continues only on the Watt/m<sup>2</sup> images.

In each thermogram, the image of the source was segmented, and a mean value for the segmented area was calculated (see Figure 6).

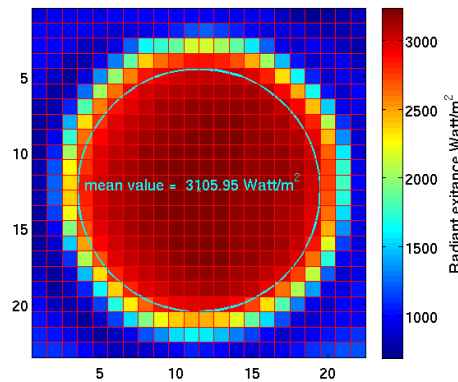


*Figure 6: Segmentation of the source and calculation of the mean value*

**CALIBRATION**

The correspondence between the temperature values measured by the temperature probes and the radiation values measured by the thermo camera had to be evaluated. During this calibration process, the temperature of the “Hohlraumstrahler” was altered several times in a wide range between 100°C and 320°C, in order to stretch a calibration curve. The temperature of the “Hohlraumstrahler” was measured in the first small drill on the side, closest to the heating element, while the thermo camera measured the radiant exitance exiting from the large drill at the end of the object. Displaying the radiant exitance in function of the probe’s temperature, the calibration curve appeared (see Figure 7). Observing the calibration curve closely, it can be seen that it consists of several more or less overlaying segments. In order to get a continuous function that describes the temperature-radiant exitance relationship, a 4<sup>th</sup> grade polynomial, according to the Stefan-Boltzmann law, was fitted onto the measurement data. This polynomial function is the calibration function for the given measurement arrangement. If some parameters of the system, like the distance between the camera and the source is changed, a new calibration is needed, which results a different curve.

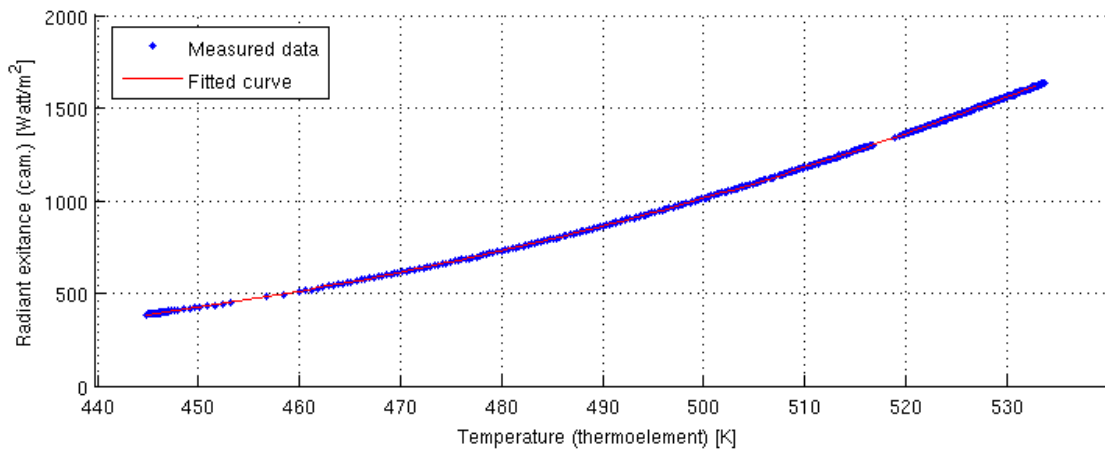


Figure 7: Calibration curve: radiant exitance measured by the thermocamera vs. temperature of the probe

The difference between the calculated calibration curve and the measured data can be calculated in order to evaluate the uncertainty for the later radiation measurements (see Figure 8).

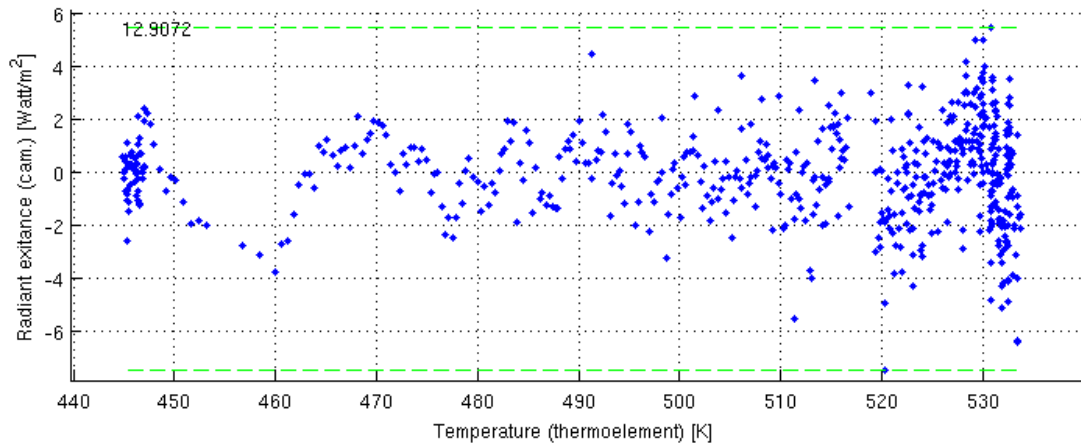


Figure 8: Evaluation of the measurement uncertainty: difference between the measured values and the calibration curve

## REFLECTIVITY MEASUREMENT

After calibrating the measurement setup, the reflectivity measurements could be done. The source and the camera were set in a different position: both of them directed to the measured surface, closing a small angle, about  $10^\circ$  between their axes, resulting in a  $5^\circ$  incident angle. A smaller angle couldn't be reached without using additional mirrors and/or expansion of the optical path, due to the physical dimensions of the camera and the source.

The length of the optical path from the source to the object and then to the camera was the same as in the case of the calibration. The lay of the anisotropic objects was fixed in such a way that the grooves of the surface, due to the machining, were perpendicular to the plane of reflection. Each object was measured for 60 seconds at a 1Hz measurement rate, resulting in 60 measurements from which a mean value and a deviation range was calculated.

The measured data was processed according to the method described earlier. For each camera measurement, the intensity of the source's radiant exitance was calculated according to the calibration curve. The quotient of the camera measurement and the source's radiant exitance gives the reflectance of the surface in the camera's spectrum. In Figure 10, the results of the measurements can be seen compared to the predictions by the theoretical model. Since the thermocamera works on wide wavelength range, the theoretical expected values were calculated for the lower and upper wavelength limits ( $\lambda_1$  and  $\lambda_2$ ) of the camera, similarly the limits due to the Rayleigh criterion (Equation 3) were also indicated for both wavelengths. At each measured object, the uncertainty of the measured roughness and the reflectance is indicated.

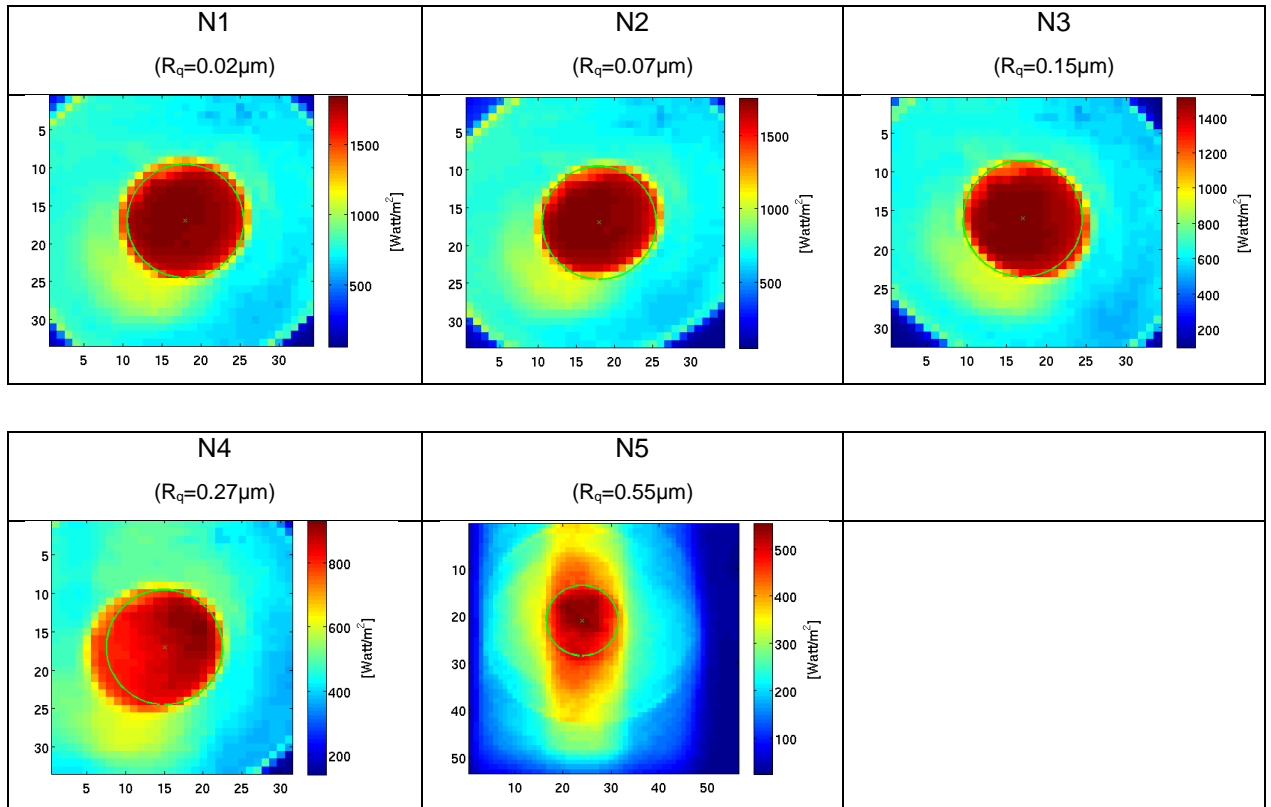


Figure 9: Reflected images of the radiation source from surfaces with different roughness

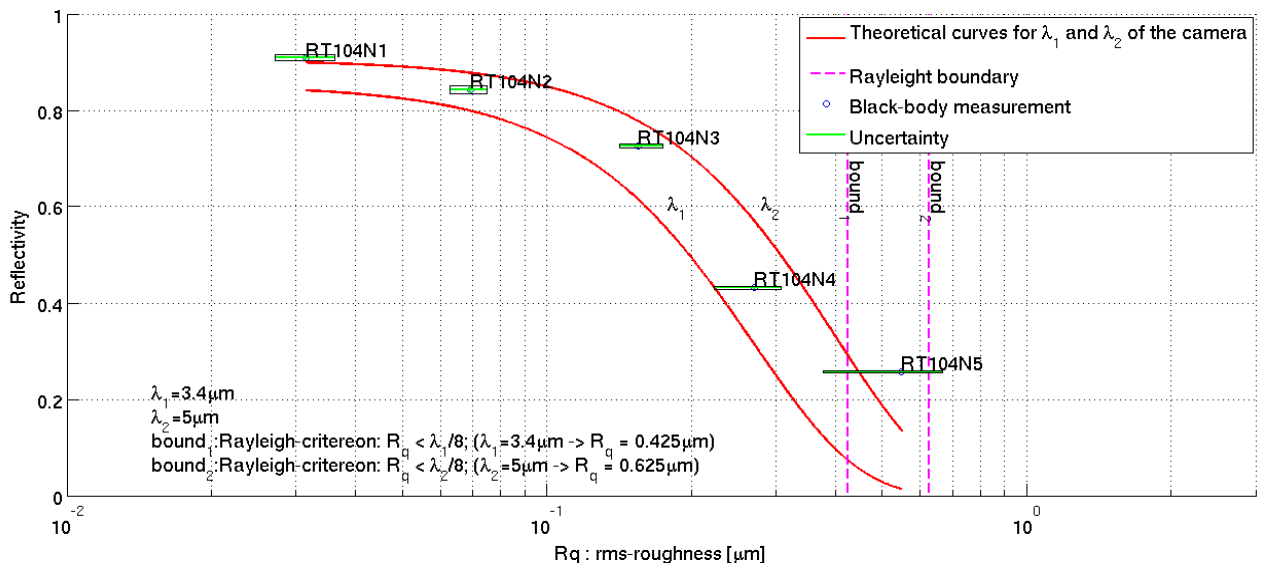


Figure 10: Measured reflectivity from plane ground parts with different surface roughnesses compared to the theoretical model of Bennett and Porteus [2], also indicating the limits defined by the Rayleigh-criterion for the 2 wavelength limits of the camera.

The results generally show a good coincidence with the theoretically predicted data, though there are some differences. In case of object RT104N5, the surface roughness was larger than the 1/8<sup>th</sup> of the wavelength (Rayleigh criterion), thus the measured irradiance was higher due to the additional scattered intensities. In case of the smoothest surface RT104N1, the evaluated reflectivity is slightly higher than the expected value. This could be due to the fact that for the calculation of expected material reflectivity iron was used instead of

hardened steel, resulting in a slightly higher reflectivity. Unfortunately, no reflectivity data was available for the given alloy in the literature.

Figure 11 shows the results in the case of the aluminum sheet parts. Large deviations can be observed for part “alu\_01” and “alu\_02”. These parts had an unusual thick oxide layer on the aluminum part. The transmissivity of aluminum-oxide is very low in the infrared range, thus an artificial, thick layer of it reduces the incident and the reflected radiation considerably. After removing the original, thick oxide layer by polishing the parts, a natural, thinner oxide layer developed immediately, resulting in values (“alu\_21”, “alu\_22”) much closer to the expected ones. In case of the parts “alu\_06”, “alu\_ac170”, “alu\_6016” and “alu\_5182” the roughnesses of the surfaces were higher than the boundary defined by the Rayleigh-criterion, similarly to the case of “RT104N5” in the previous dataset.

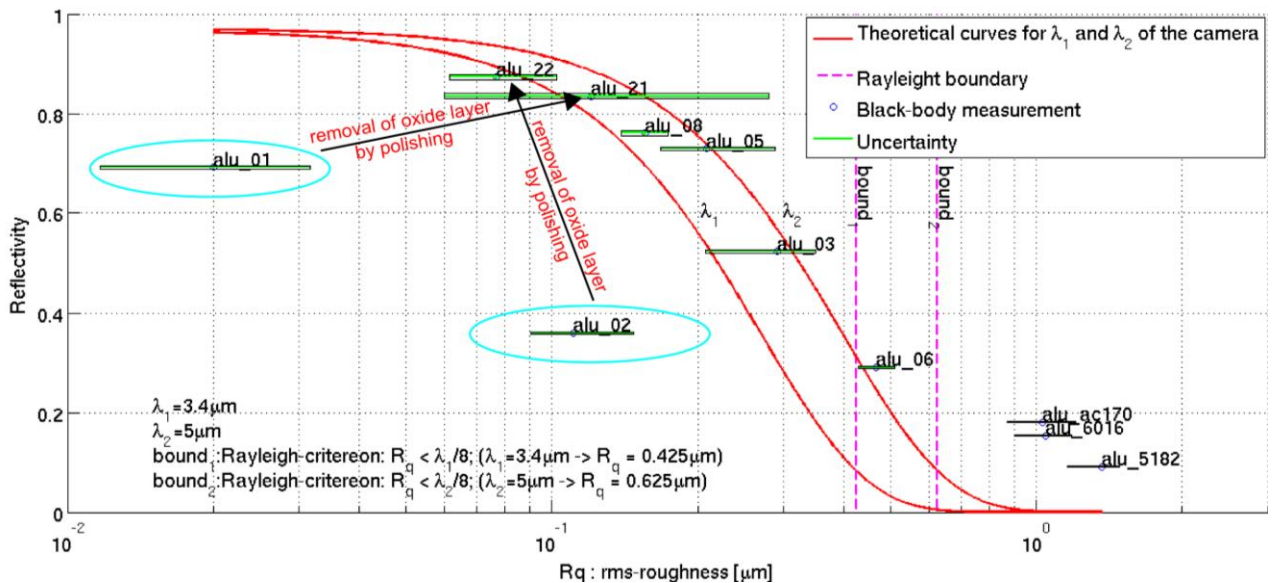


Figure 11: Measured reflectivity from aluminum sheet parts with different surface roughnesses compared to the theoretical model of Bennett and Porteus [2], also indicating the limits defined by the Rayleigh-criterion for the 2 wavelength limits of the camera.

## SUMMARY AND OUTLOOK

We measured the specular reflectance of different metal surfaces in the MWIR spectrum using a thermo camera and a calibrated source. The results of the measurement show a good correlation with the theoretical model of Bennett and Porteus [2]. The specular reflectance of the surfaces is reduced with the increased surface roughness of the test object. This method can be used under certain conditions. The surface roughness of the object should obey the Rayleigh smoothness criterion: the RMS-roughness should be at least 8 times smaller than the wavelength of the light, i.e. working spectrum of the camera, otherwise the irradiance contains a considerable amount of scattered intensity, resulting in false results.

In order to improve the measured results, the following changes are planned in the measurement process. A different theoretical model, for example the He-Torrance-Sillion-Greenberg [2] model will be used instead of the current one, to have more accurate predictions. The geometry of the cavity of the source can be further optimized, by making the opening smaller than the inner cross-section, to improve the emissivity. By the application of a thermally decoupled aperture in front of the cavity's opening, the unwanted increase in the reflected irradiance in case of rough surfaces can be reduced, due to the decreased intensity of the scattered irradiance from the cavity's environment. A source with stabilized temperature is also planned by thermally isolating the outer surface of the source. The position of the temperature probe will be even closer to the bottom of the cavity. By using a finite element (FEM) simulation of the source (see Figure 12), the distribution of the temperature in source object can be better understood, thus the calibration can be further improved.

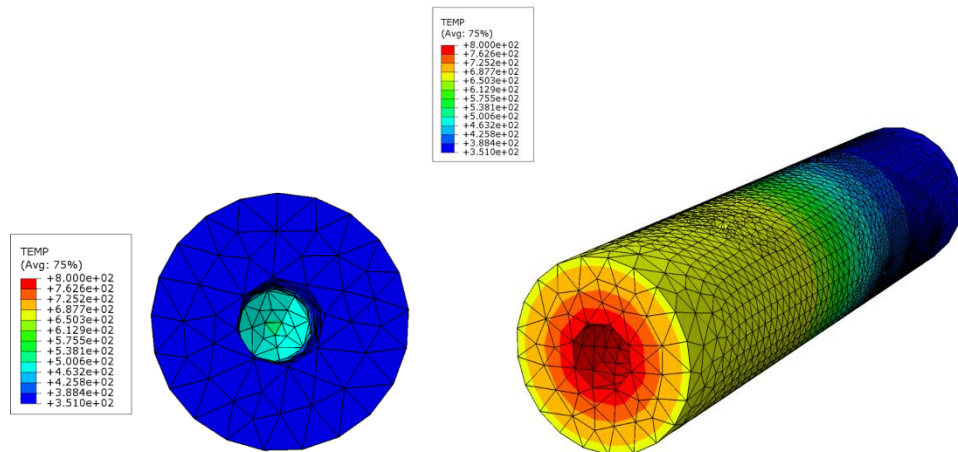


Figure 12: FEM simulation of the temperature distribution in the source object

## REFERENCES

- [1] H. E. Bennett and J.O. Porteus. Relation between surface roughness and specular reflectance at normal incidence. *Journal of the Optical Society of America*, 51:123-129, 1961.
- [2] He XD, Torrance KE, Sillion FX, Greenberg DP. A comprehensive physical model for light reflection. *ACM SIGGRAPH Computer Graphics*. 1991;25(4):175-186.
- [3] Paquin R. Properties of metals. In: Bass M, Stryland EW, Williams DR, Wolfe WL *Handbook of Optics, Volume II: Devices, Measurements, and Properties*. Vol 2. second. McGraw-Hill; 1995:35.1-35.78.
- [4] Sarosi Z, Knapp W, Kunz A. Detection of surface defects on sheet metal parts by using one-shot deflectometry in the infrared range. *Proceedings of InfraMation2010*, 210-160-Sarosi
- [5] ISO 4288:1996(E). Geometrical Product Specifications (GPS) – Surface texture: Profile method- Rules and procedures for the assessment of surface texture.
- [6] Anthony J. LaRocca. *The infrared handbook*; chapter 2 Artificial sources. Environmental Research Institute of Michigan, revised edition, 1989
- [7] Robert P. Beault. *Handbook of optics, volume 2 Devices, Measurements and Properties*, chapter 37 Black surfaces for optical systems, pages 37.1-37.70. McGraw-Hill Professional, second edition, 1995.
- [8] Bernd Schonbach. *Bildverarbeitung und optische Messtechnik in der industriellen Praxis*, chapter 2 Warmebildkameras und IR-Bildverarbeitung, pages 21-53. Franzis-Verlag, Munchen, 1993

## ABOUT THE AUTHOR

The author received his MSc. degree in informatics in 2001 at the University of Miskolc, Hungary. He is currently working on his PhD. thesis in the field of optical metrology at the ETH Zurich in Switzerland while working for the inspire AG in Zurich. His main fields of interests are image processing, simulations and 3D optical measurement.